



Article

# Multi-Source Based Spatio-Temporal Distribution of Snow in a Semi-Arid Headwater Catchment of Northern Mongolia

Munkhdavaa Munkhjargal <sup>1,\*</sup>, Simon Groos <sup>2</sup>, Caleb G. Pan <sup>3</sup>, Gansukh Yadamsuren <sup>4</sup>, Jambaljav Yamkin <sup>4</sup> and Lucas Menzel <sup>1</sup>

<sup>1</sup> Professorship in Hydrology and Climatology, Department of Geography, Heidelberg University, Im Neuenheimer Feld 348, 69120 Heidelberg, Germany; lucas.menzel@uni-heidelberg.de

<sup>2</sup> Faculty of Spatial Information, Dresden University of Applied Sciences, Friedrich-List-Platz 1, 01069 Dresden, Germany; Simon.Groos@hotmail.de

<sup>3</sup> Numerical Terradynamic Simulation Group, University of Montana, Missoula, MT 59812, USA; Caleb.Pan@mso.umt.edu

<sup>4</sup> Permafrost Laboratory, Institute of Geography and Geoecology, Mongolian Academy of Science, Erkhuu Street, Sukhbaatar District, Ulaanbaatar UB-14192, Mongolia; gansukh.khatan@gmail.com (G.Y.); jambaljav@gmail.com (J.Y.)

\* Correspondence: munkhjargal@uni-heidelberg.de; Tel.: +49-6221-54-5571

Received: 6 December 2018; Accepted: 14 January 2019; Published: 19 January 2019



**Abstract:** Knowledge of the duration and distribution of seasonal snow cover is important for understanding the hydrologic regime in mountainous regions within semi-arid climates. In the headwater of the semi-arid Sugnugur catchment (in the Khentii Mountains, northern Mongolia), a spatial analysis of seasonal snow cover duration (SCD) was performed on a 30 m spatial resolution by integrating the spatial resolution of Landsat-7, Landsat-8, and Sentinel-2A images with the daily temporal resolution of Moderate Resolution Imaging Spectroradiometer (MODIS) snow products (2000–2017). Validation was achieved using in situ time series measurements from winter field campaigns and distributed surface temperature loggers. We found a mean increase of SCD with altitude at approximately +6 days/100 m. However, we found no altitude-dependent changes in snow depth during field campaigns. The southern exposed valley slopes are either snow free or covered by intermittent snow throughout the winter months due to high sublimation rates and prevailing wind. The estimated mean SCD ranges from 124 days in the lower parts of the catchment to 226 days on the mountain peaks, with a mean underestimation of 12–13 days. Snow onset and melt dates exhibited large inter-annual variability, but no significant trend in the seasonal SCD was evident. This method can be applied to high-resolution snow mapping in similar mountainous regions.

**Keywords:** snow; snow cover duration; persistent and intermittent snow; optical remote sensing; northern Mongolia

## 1. Introduction

The duration and distribution of snow cover is an important governor of hydrologic and ecologic processes and contributes a significant role in local and regional hydrologic regimes [1–3]. For basin headwaters in arid or semi-arid regions, seasonal snow-melt sustains river discharge, contributing to regional water resources during dry summer periods. Hence, accurate estimation of snow cover area (SCA) is needed to evaluate the runoff from snowmelt. Snow cover also plays an important role in permafrost distribution through its insulating effect on seasonal ground temperature [4]. In response to recent accelerated warming, there has been an observed decrease in SCA and snow cover duration

(SCD) in the Arctic regions [5]. In the mid-latitudes of Central Asia, snow cover has been observed to accumulate later into the autumn season [6] whilst the spring melt period coincides with increasing spring rainfall [7], reflecting mid-latitude extreme weather in winter months, coinciding with the arctic amplification and the strengthening of the Siberian high (SH) [8,9]. The SH creates an extreme continental climate that promotes low temperatures and longer seasonal snow cover extent, and is centrally located over northern Mongolia [10]. Our understanding of the timing and characteristics of snow cover is highly limited, yet it is critical, as Mongolia's climate is semi-arid, largely governed by the SH.

Snow cover can be accurately monitored using in situ measurements, including snow depth, density, and snow water equivalent (SWE); however, such measurements are limited for broad spatial analyses due to their sparse monitoring networks. In contrast, optical remote sensing applications are capable of detecting SCA globally with frequent temporal coverage but are often limited by cloud cover and winter time solar darkness.

Optical remote sensing data provide one of the best opportunities to characterize SCA and SCD in the data scarce region of Mongolia due to a high number of clear sky days during winter, promoted by the SH. The Moderate Resolution Imaging Spectroradiometer (MODIS) has provided daily snow cover products with 500 m spatial resolution since 2000, including MODIS Terra (MOD10A1) and Aqua (MYD10A1) [11–17]. In addition to MODIS, other popular optical sensors exist, including the Landsat series and more recently, the Sentinel-2A series, providing a higher spatial resolution but at a reduced temporal resolution [18], relative to MODIS. The combination of MODIS, Landsat, and Sentinel images [19] have proven to be useful to retrieve SCA by applying different downscaling techniques using air temperature, solar radiation, and topography [20–22]. However, the effectiveness in detecting SCA and SCD by such optical sensors is challenged by landscape heterogeneity created by topography, patchy snow cover, forest canopy, cloud coverage, and the spatial and temporal resolutions [13,23].

In this study, we combine the daily temporal resolution of MODIS Terra and Aqua with the high spatial resolution of Landsat and Sentinel images to derive SCA and SCD at a 30 m spatial resolution and at a daily temporal resolution over the Sugnugur catchment in northern Mongolia for winters 2000/2001 to 2016/2017. The catchment area (495 km<sup>2</sup>) is located about 100 km northwest of Ulaanbaatar in northern Mongolia (Figure 1), with elevations ranging from 960 to 2800 m.a.s.l., forming the headwaters of the Selenga River before it drains into Lake Baikal. The importance of this small headwater catchment is highlighted for its snow-melt water contribution to regional water resources and energy exchange balance. Approximately 30% of the annual precipitation occurs as snowfall during the winter months [24,25], and 20% of annual evapotranspiration comes from snow sublimation and snow-melt water [26,27]. North-west prevailing winds are dominant and bring the majority of the precipitation, with a strong orographic effect. The lower elevations are defined by shrubs with short grasslands, whilst the Siberian boreal forest is found on north-facing slopes and higher elevations; yet about one third of this forest cover has been affected by wildfires [25].

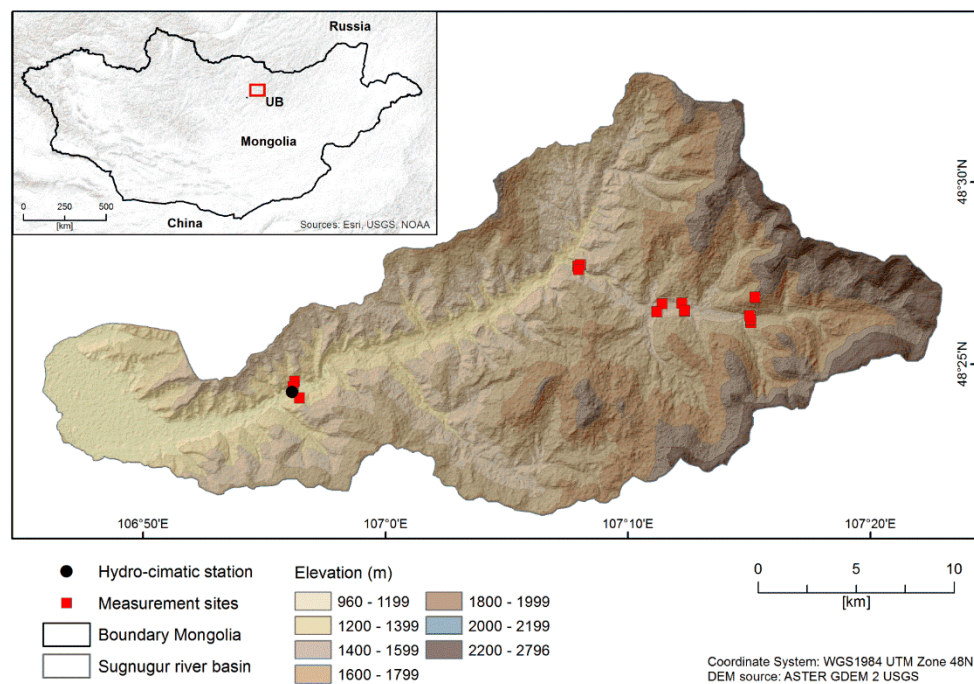


**Figure 1.** Sugnugur river catchment. Red points indicate the locations of snow field campaigns, as well as the surface temperature measurements. The hydro-climatic station is located at elevation 1193 m.a.s.l. UB is Ulaanbaatar.

We quantified the spatial distribution and timing of seasonal snow cover (i), introduced an alternative correction method to account for elevation and land cover when detecting SCA and SCD (ii), and reconstructed the snow cover development over the winter 2016/2017 (iii). We validated our results using several in situ observations including surface temperature, snow field measurements, and time-lapse photographs.

## 2. Materials and Methods

### 2.1. Materials

We used daily MODIS Terra (MOD10A1 V.006) and Aqua (MYD10A1 V.006) snow products (i), a digital elevation model (DEM) with 30 m spatial resolution (ii), Landsat-7, Landsat-8, and Sentinel-2A data (iii), a Landsat based land-cover classification map (iv), hydro-climatic data observed with high frequency (v), iButton surface temperature measurements distributed in the catchment (vi), and photographs from a time-lapse digital camera (vii). The datasets i–iv were used for reconstructing SCA and SCD whereas v–vii were used to validate the results.

**MODIS snow-cover data:** Daily MODIS snow products (Version. 006) from the Aqua and Terra satellites with 500 m spatial resolution were employed for the winters 2000/2001 to 2016/2017. These products contain normalized difference snow index (NDSI) values 0–100 as percentages, as well as other parameters, including cloud coverage. The MODIS snow products including the 8-day composite snow product are also widely used in many regions of the world [28–38]. However, the main drawbacks of these products are cloud coverage and coarse spatial resolution [39]. Therefore, we used the original daily data rather than using 8-day snow product to minimize the uncertainties that may have resulted from any cloud-filtering [15]. The data were obtained from the National Aeronautics and Space Administration (NASA) Earth Observing System Data and Information System (EOSDIS) Reverb platform [40].

**Digital Elevation Model:** We used a 30 m DEM derived from the Advanced Spaceborne Thermal Emission and Reflection Radiometer (ASTER) [41]. The DEM was used to derive the altitude-dependent rate of SCD to aggregate MODIS data to 30 m resolution.

**Landsat and Sentinel data:** Optical remote sensing data from the Landsat-7, Landsat-8, and Sentinel-2A were used to generate the winter snow cover time series [42]. The Landsat-7/8 data have a spatial resolution of 30 m and a temporal resolution of 16 days (8 days when they are combined). The Sentinel-2 has a spatial resolution of 20 m and a temporal resolution of 5 days. In total, 40 clear-sky day images (Table S1, Supplementary Materials) between the beginning of October 2016 (mid-autumn) and end of May 2017 (late spring) were processed. The Sentinel images were aggregated to 30 m resolution to meet the same Landsat and DEM resolutions.

**Land-cover:** Land-cover classification for Sugnugur catchment was produced based on a Landsat-7 image of the year 2011. We believed that this map was appropriate because there was no significant change in land-cover since 2011. In total, five different land-covers were classified in the Sugnugur catchment, including: forest, burned forest, short grassland, shrub, and rock. Areas with forest and shrubs were used in this study for correcting snow distribution maps from the Landsat and Sentinel images because of the low snow detection rate under canopy closure.

**In-situ measurements:** Snow depth (SD) has been observed using the Campbell SR50A-L sensor since winter 2012/2013 in short grassland vegetation, as well as other climatic parameters such as precipitation, air temperature, surface temperature, and albedo at our hydro-climatic station site located near the entry of the catchment. The SD sensor measures the distance between the sensor and the underlying surface. These data contain continuous SD measurements including records on no-snow conditions with 1 h intervals. As the snow depth measurement at the hydro-climatic station site cannot represent the areal distribution of snow in the catchment, we also conducted a series of snow field measurements at 13 locations for two consecutive winters, 2016–2018, in order to understand the spatial variability of snow distribution and SD. In addition to the snow field measurements, we also observed surface temperatures for 2016–2017 using temperature iButtons at near surface (5 cm) depth with a 3 h interval. The iButtons were placed at all the snow field measurement locations with altitudes ranging from 1193 to 1612 m.a.s.l.

## 2.2. Methods

The main idea of the methodology applied in this study was to downscale the coarse resolution MODIS data based on a combination of other freely available optical remote sensing images, as well as ground measurements. An altitude-dependent SCD rate derived from MODIS data and DEM coupled with snow cover area (SCA) derived from the combination of Landsat and Sentinel images were used to produce annual SCD maps with 30 m spatial resolution from 2000–2017. We used the daily temporal resolution of MODIS Aqua and Terra satellites for deriving the temporal distribution of snow over the last 17 years, particularly the altitude dependent SCD rate, snow onset ( $S_o$ ), and melt ( $S_m$ ) dates. The Landsat and Sentinel images, with high spatial resolutions, were used for constructing the spatial distribution of snow in the study area. The abbreviations used in this study are shown in Table A1, Appendix A, and the flowchart of the procedure can be found in Figure 2.

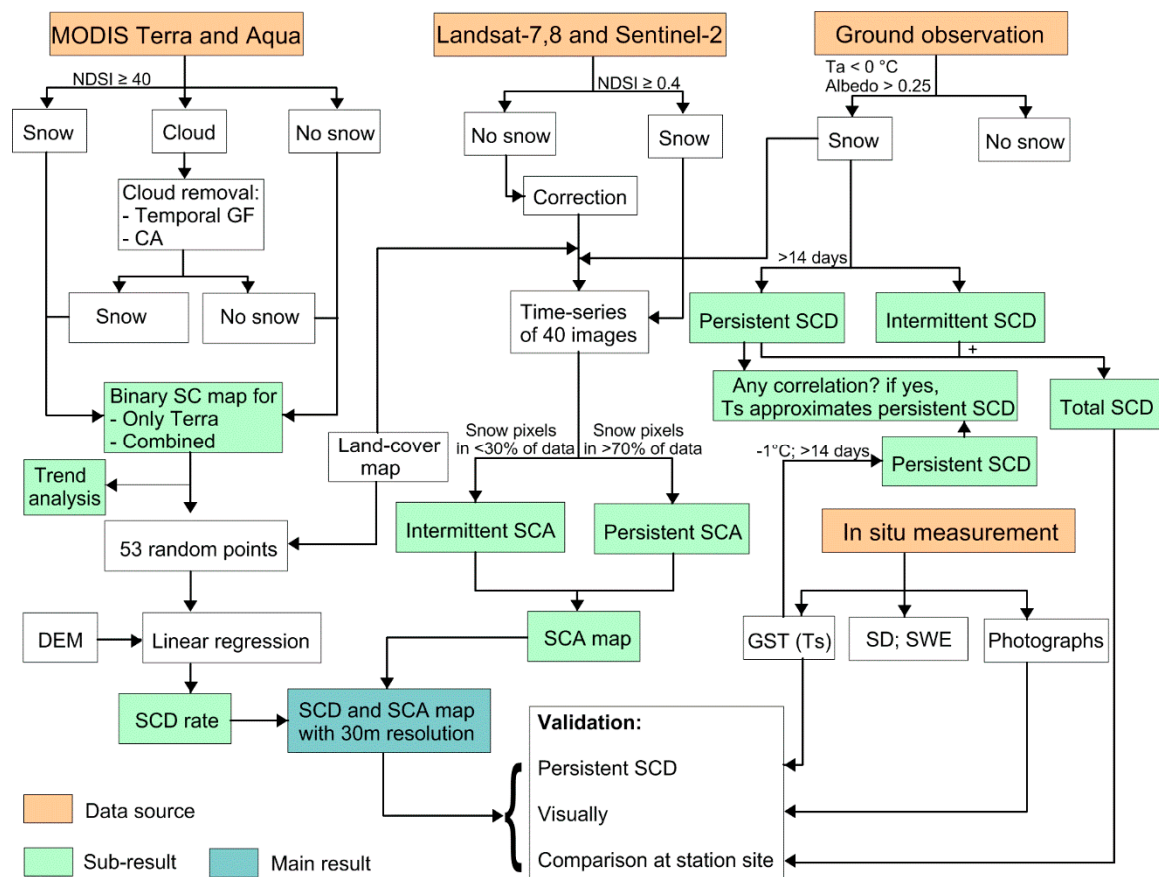


**Figure 2.** Flowchart of the procedure to map snow cover duration (SCD) and snow cover area (SCA) in the Sugnugur catchment. MODIS is Moderate Resolution Imaging Spectroradiometer. NDSI is normalized difference snow index. GF and CA are gap-filling and conditional adjustments, respectively.  $T_s$  and  $T_a$  denote daily mean ground surface temperature (GST) and daily mean air temperature, respectively. SD and SWE are snow depth and water equivalent, respectively.

For all satellite images, we adopted the normalized difference snow index (NDSI) with a threshold of  $\geq 0.4$  to denote snow cover [40,42–44].

$$NDSI = \frac{Green - SWIR}{Green + SWIR} \tag{1}$$

where *Green* represents reflectance in a visible band and *SWIR* is reflectance in a short-wave infrared band.

*Estimating SCD from ground temperature:* The timing characteristic of snow cover was studied at the hydro-climatic station to understand the general snow accumulation and ablation processes in the study area. SCD is commonly derived from SD, SWE, or satellite data. In this study, a daily mean air temperature ( $T_a$ ) of  $< 0\text{ }^\circ\text{C}$  and a daily mean albedo of  $\geq 0.25$  (unitless) were used to distinguish snow from the existing vegetation (Figure 3). We assume a persistent snow cover (continuous) if these two conditions are consistent for at least 14 days, otherwise it will be assigned as intermittent (not continuous). Occasional autumn and spring (transition periods) snowfalls develop intermittent snow cover lasting for a couple of days, whereas decreased air temperature towards the winter months (DJF) allows the snow cover to become persistent. We classified snow duration for each year as the sum of both intermittent SCD and persistent SCD.



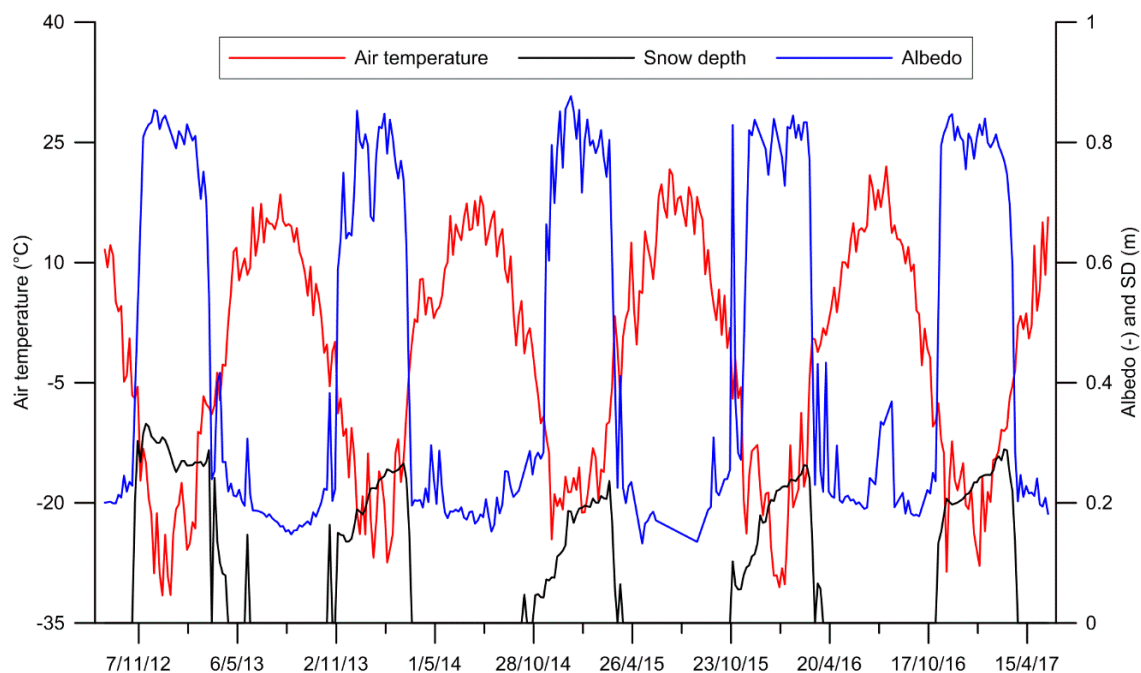


**Figure 3.** Snow depth (SD) collected from the SR50A-L sensor at the hydro-climatic station site by coupling with daily air temperature and albedo. The values are shown as 5-day averages.

We also used surface temperatures collected from the hydro-climatic station as proxies to classify persistent snow cover, such that if the daily mean surface temperature ( $T_s$ ) remained below  $-1\text{ }^{\circ}\text{C}$  for at least 14 days, the snow cover was determined as persistent. These conditions were then applied to our iButton measurements, which allowed us to validate our reconstructed SCD across the catchment. We examined the sign and strength of the relationship between the persistent SCD determined from the  $T_a$  and albedo and that approximated from  $T_s$  using Pearson's correlation. We assumed that if a positive and significant relationship existed, then persistent SCD may be reconstructed from  $T_s$ . Winter 2012/2013 was an exceptional year with relatively low temperatures in autumn, which led to a high number of below  $-1\text{ }^{\circ}\text{C}$  days. Therefore, we did a manual correction by selecting the days between the date when first snowfall was observed after the surface temperature dropped below the threshold and the date when albedo dropped to below 0.25.

*MODIS derived snow metrics:* The timing characteristic of snow over the study area was analyzed using the daily MODIS Terra and Aqua data by determining snow onset ( $S_o$ ) and snow melt ( $S_m$ ) dates, as well as SCD for snow seasons 2000–2017. We first separated the cloudy pixels, designated with a value of 250, from the cloud free pixels and then detected the snow cover for the cloud free pixels using the NDSI to create daily 500 m snow maps.

To reduce cloud coverage, we applied a series of cloud removal approaches to Terra and the combination of Terra and Aqua data separately. First, we applied a 1-day backward and forward gap-filling (temporal GF) approach, with a limit of 3 days, to both Terra and Aqua such that when a pixel is cloudy, it goes one day backward and forward to test for a cloud free pixel [11,44]. Following this temporal gap-filling, a conditional adjustment (CA), which takes spatial and seasonality corrections into account, was applied. The CA assumes that if the given pixel after the temporal gap-filling is still cloudy, it can be reclassified as snow or no-snow under certain circumstances; if two of the 8-neighboring pixels at lower elevation are cloud free and the day of year is within the range between  $S_o$  and  $S_m$  dates of that certain pixel, we assigned snow. The  $S_o$  and  $S_m$  dates were determined for each MODIS pixel as the first and the last day of the classified snow cover days within the hydrologic year; it also defined the length of snow season for each pixel.

After adjusting for cloud cover, gap-filled images from both Terra and the combination data still underestimated SCD over heterogeneous topography and forested areas because the coverage area

of a single  $500 \times 500$  m MODIS image includes a high range of elevations as well as both forested north- and steep south-facing slopes. Thus, we generalized the annual number of SCD from the MODIS data for each year over the study area based on annual SCD rates. To do so, 53 random points were selected, either on mountain peaks or lowland areas where no forests or shrubs exist and the topography is homogenous, in order to employ linear regression analysis between the SCD from the improved MODIS data and DEM; later the regression parameters were used for deriving the SCD rate for each year.

Trend analysis using linear least squares regression were also conducted for snow onset ( $S_o$ ), snowmelt ( $S_m$ ) dates, and SCD from the improved MODIS daily snow-cover. Since air temperature is one of the main parameters that drives the snow accumulation and ablation processes, we calculated a trend analysis for monthly mean air temperature during the snow season, using observations from the nearest long-term climate station at Chinggis Khan International Airport (60 km south from the hydro-climatic station). The results can be found in Section 3.2.2.

*Landsat and Sentinel images to correct for land-cover and topography:* The generalized SCD is not realistic because it includes the intermittent SCA, which mostly occurs on the steep south-facing slopes and wind-blown surfaces. To identify these areas, we created a sequence of snow cover maps from the combination of Landsat-7, Landsat-8, and Sentinel-2A images (40 images in total) taken on clear-sky days. These time sequence maps are helpful in showing the development of SCA with high spatial resolution in the study area. Although the spatial resolutions of the satellites are high, snow cover below the forest canopy and dense shrub is difficult to detect [45]. Therefore, a correction method, which considers altitude dependency and land-cover types, was applied to all Landsat and Sentinel images to correct snow cover in those areas. More specifically, if a pixel from either a Landsat or Sentinel image was classified as snow at the hydro-climatic station, the areas in higher elevations with forests or shrubs were also classified as snow. If not, this assumption was ignored. By repeating this correction for each image, the change detection analysis was completed for the snow season period 2016–2017, representing the development of SCA in the catchment. Based on the changes in SCA, we separated the study area as persistent SCA (pixels classified as snow in >70% of the data) and intermittent SCA (pixels classified as snow in <30% of the data). The result can be found in Section 3.3. We assumed that the general spatial distribution of snow would be similar for each year to obtain the mean SCD for winters 2000/2001 to 2016/2017 over the seasonal persistent SCA by using the empirical altitude-dependent SCD rates that were found from the improved MODIS data.

*Result assessment:* To validate the results, we first compared the estimated total SCD with the observed total SCD at the hydro-climatic station. Daily surface temperature measurements ( $T_s$ ) from the iButtons, distributed in the catchment, were also used by comparing the linear relationship, which was found at the hydro-climatic station, to that between the estimated persistent SCD days and days with  $< -1$  °C of  $T_s$  from the iButtons (Figure 2). Photographs from the time-lapse camera and snow field measurements were also used to verify the spatial distribution of snow visually.

### 3. Results

#### 3.1. Seasonal Snow Cover from In Situ Measurements

In general, seasonal snow cover lasts from the beginning of October until the end of March with strong variability during the transition period. This transition period refers to late autumn and early spring with occasional intermittent snowfalls that develop a non-continuous snow cover that is relatively thin and temporary. Observed snow depth derived with the combination of  $T_a < 0$  °C and albedo  $\geq 0.25$  showed that the total SCD ranged from 145 to 157 days with a mean depth of 12–25 cm/year from 2012–2017. The intermittent and persistent snow cover days were distinguished for each year (Table 1). The duration of persistent snow cover was relatively stable while the intermittent snow cover days showed strong variability ranging from 6 to 21 days. The maximum snow depths

were observed in the second half of March before the main melt started. There was no clear relationship between the variability of snow depth and the duration of snow cover.

**Table 1.** Intermittent and persistent snow cover days (SCD) during the observation period. <sup>1</sup> and <sup>2</sup> denote the persistent SCD derived from the combination of albedo and air temperature and below  $-1\text{ }^{\circ}\text{C}$  of daily mean surface temperature, respectively.

	2012/13	2013/14	2014/15	2015/16	2016/17
Intermittent	13	12	13	21	6
Persistent	132 <sup>1</sup> /140 <sup>2</sup>	135 <sup>1</sup> /135 <sup>2</sup>	144 <sup>1</sup> /143 <sup>2</sup>	137 <sup>1</sup> /139 <sup>2</sup>	141 <sup>1</sup> /147 <sup>2</sup>
Total	145	146	157	156	147

As snow cover influences the surface energy balance significantly [46], the temperature at the underlying surface can serve as a proxy of absence and presence of seasonal persistent snow cover. Therefore, we validated persistent SCD using  $T_s$  at several locations, where snow cover was underestimated from MODIS sensors, and which is demonstrated in Figure 4 by plotting snow depth together with surface temperature measurements for each year at the hydro-climatic station.

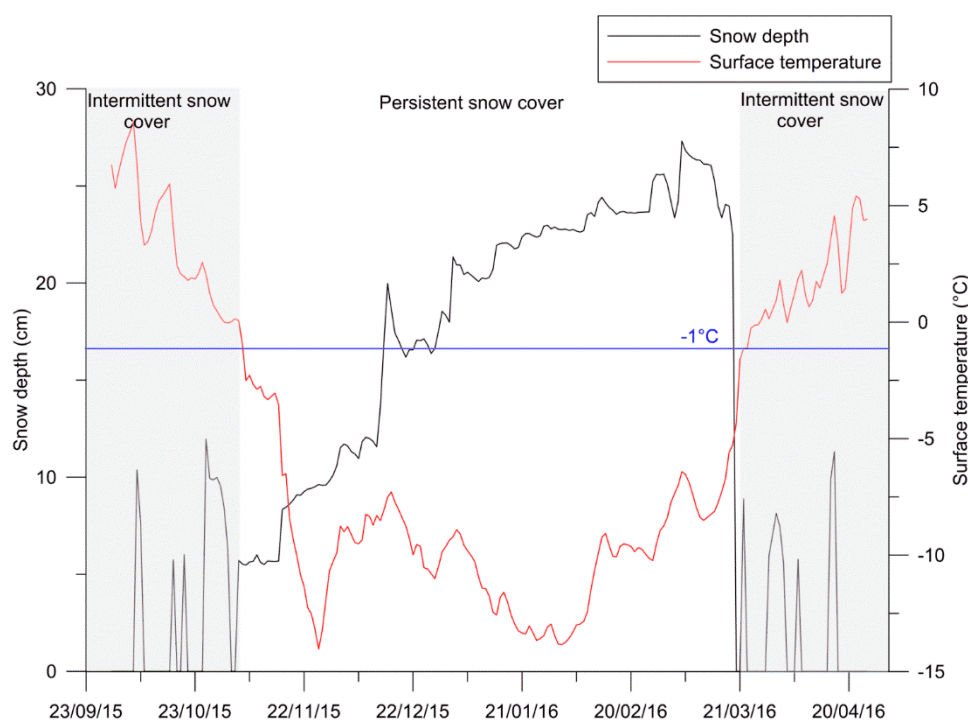


**Figure 4.** An example of the discrimination of intermittent and persistent snow cover, determined from the combination of albedo and air temperature measurements. The red and blue lines indicate the observed daily mean surface temperature and the threshold of  $-1\text{ }^{\circ}\text{C}$ , respectively. The black line describes the typical snow accumulation during the snow season.

For the observation period at the hydro-climatic station, the distinguished persistent SCD showed a moderate and positive correlation ( $r = 0.64$ ,  $p < 0.05$ ) with the persistent SCD determined from the surface temperature record. These results suggest further that persistent SCD in other parts of the catchment could be verified using the surface temperature iButton measurements. Snow field measurements were conducted at each iButton location, and south-facing slopes were snow free while both valley bottom and north-facing slopes had similar SD, indicating no changes with increasing altitude (see details of the snow field measurements in Table S2, Supplementary Materials).



### 3.2. Temporal Distribution of Snow

#### 3.2.1. Cloud Reduction

To reduce cloud cover in the daily Terra and the combined Aqua and Terra images, the temporal gap-filling (GF) and conditional adjustment (CA) were applied to both datasets. Figure 5 shows the results as the mean cloud coverage. The most obvious decrease appeared after the temporal GF filtering [47]. The relative percentage of cloud cover for the entire study area decreased up to 100% from the initial MODIS data to the final CA filtering. The combination of the two initial data yielded only slight improvements in reducing cloud coverage because the time difference between the two overpasses was about 3 h; hence general atmospheric conditions remained similar. The difference between Terra and the combined version after the final CA was not significant.

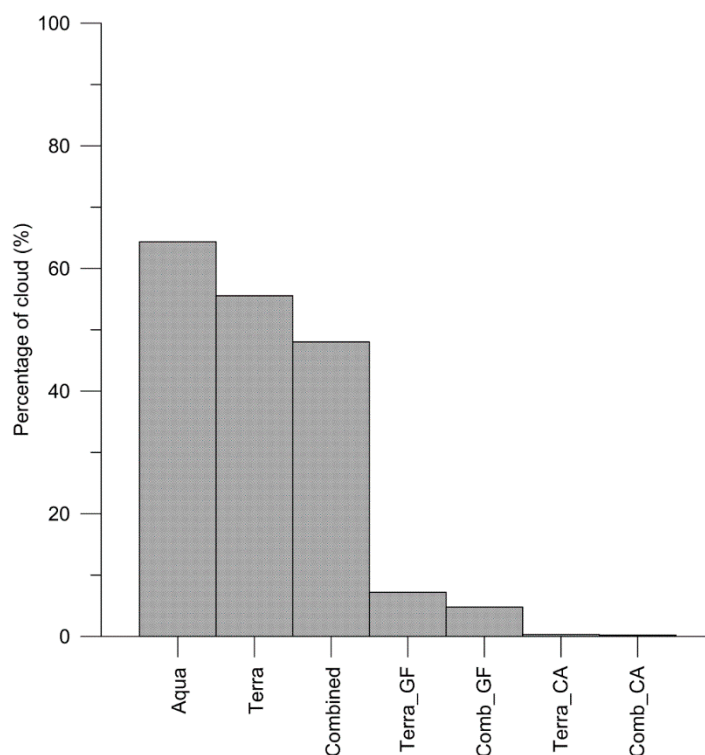


**Figure 5.** Changes in percent of cloud coverage after a series of cloud reduction steps applied to daily MODIS snow products Aqua and Terra; Combined—The combination of both satellites; Terra\_GF—Gap-filling applied to only Terra; Comb\_GF—Gap-filling applied to the combination; Terra\_CA—Conditional adjustment applied to Terra\_GF; Comb\_CA—Conditional adjustment applied to Comb\_GF.

#### 3.2.2. SCD and Trend Analysis

Altitude, latitude, and solar radiation are known factors that govern SCD as well as their spatial distribution [48,49]. Due to the study area's relatively small size, stretched from east to west, the derived SCD from the improved MODIS data showed an insignificant relationship with potential solar radiation ( $p = 0.33$ ); therefore, we ignored the influence of latitude and topography, and considered only the altitude dependency for deriving the SCD rate (days/m). The mean annual SCD ranged from 124–226 days from the lowland plain area to the mountain peak, showing clear underestimation over the forested and heterogeneous topography area (Figure 6). The mean increasing SCD rate was +6 days/100 m with mean coefficient of determination  $r^2 = 0.92$  (ranging from 0.71–0.96) with the probability value  $p < 0.001$ , and it agrees well with the result (+5.9 days/100 m) found in other Central Asian mountains [7].

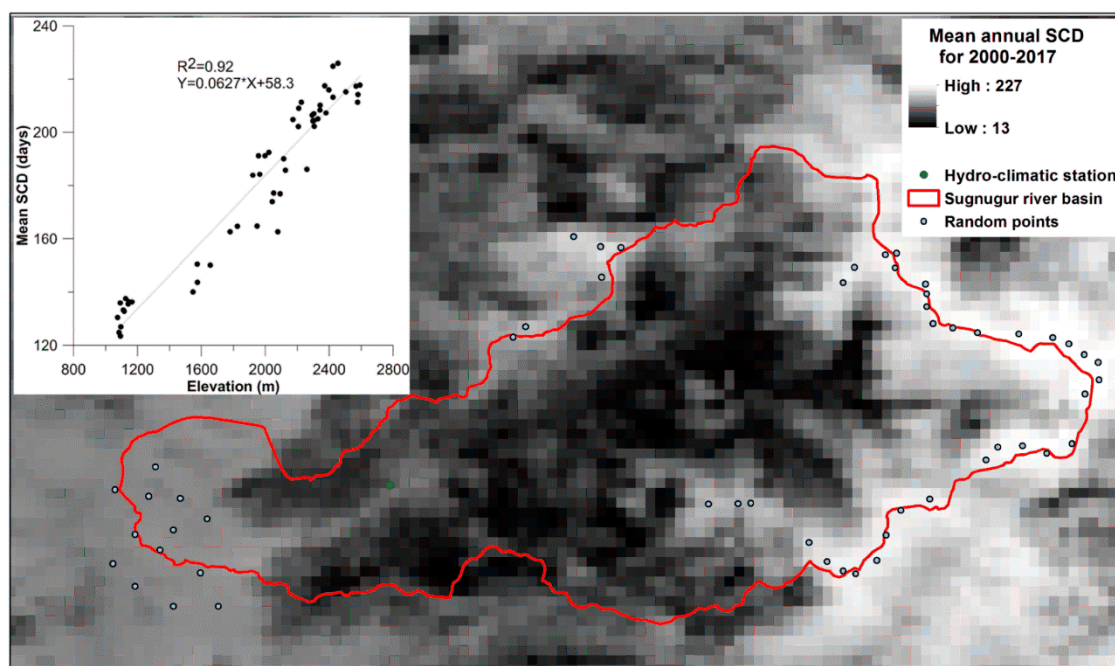


**Figure 6.** Mean annual snow cover duration (SCD) for 2000–2017 from the improved MODIS-Terra and the derived mean SCD rate (inset image). Green and blue dots denote the locations of hydro-climatic station and selected random points, respectively. Areas with heterogeneous topography and forest cover mostly in the middle part of the catchment demonstrate significant underestimation, such as only 13 days, as shown in the scale.

The trend analyses of MODIS derived snow metrics ( $S_o$ ,  $S_m$ , and SCD) and long-term air temperature of snow season (from October to April) are shown in Figure 7. The  $S_o$  and  $S_m$  dates exhibited large inter-annual variability with insignificant slightly increasing delays in both  $S_o$  ( $p = 0.53$ ) and  $S_m$  ( $p = 0.77$ ) dates, indicating a slight shift in the snow season. To implement trend analysis for the total SCD, we separated the study area into two parts (mountain and plain area) based on an elevation threshold (2300 m.a.s.l) of the tree line [25], excluding the area that is always underestimated from the MODIS data because of the forest canopies and topographic heterogeneity. Overall, the SCD over both the mountains and the plains showed insignificant decreasing trends ( $p = 0.96$  for plains and  $p = 0.41$  for mountains). The mean change rates were  $-0.5$  days/year for mountains and  $-0.04$  days/year for the plains, respectively. The mean SCD for mountain peaks dropped down to its minimum in winter 2014/2015 and increased to its maximum in winter 2012/2013. On the contrary, SCD in the plains showed high variability between 2000 and 2008, and then it stabilized. The hydrologic year 2001/2002 had the shortest SCD in the plains due to late snow cover onset and early snow melt, and is in good agreement with the other findings in Central Asia [50]. In addition, there was no decline in snow cover over our study period, which is also in an agreement with other studies in the region, e.g., [1]. Nevertheless, the time series of 17 years may be relatively short to produce a trend analysis of these snow metrics, and a longer time-series of data may be necessary for a more comprehensive analysis.

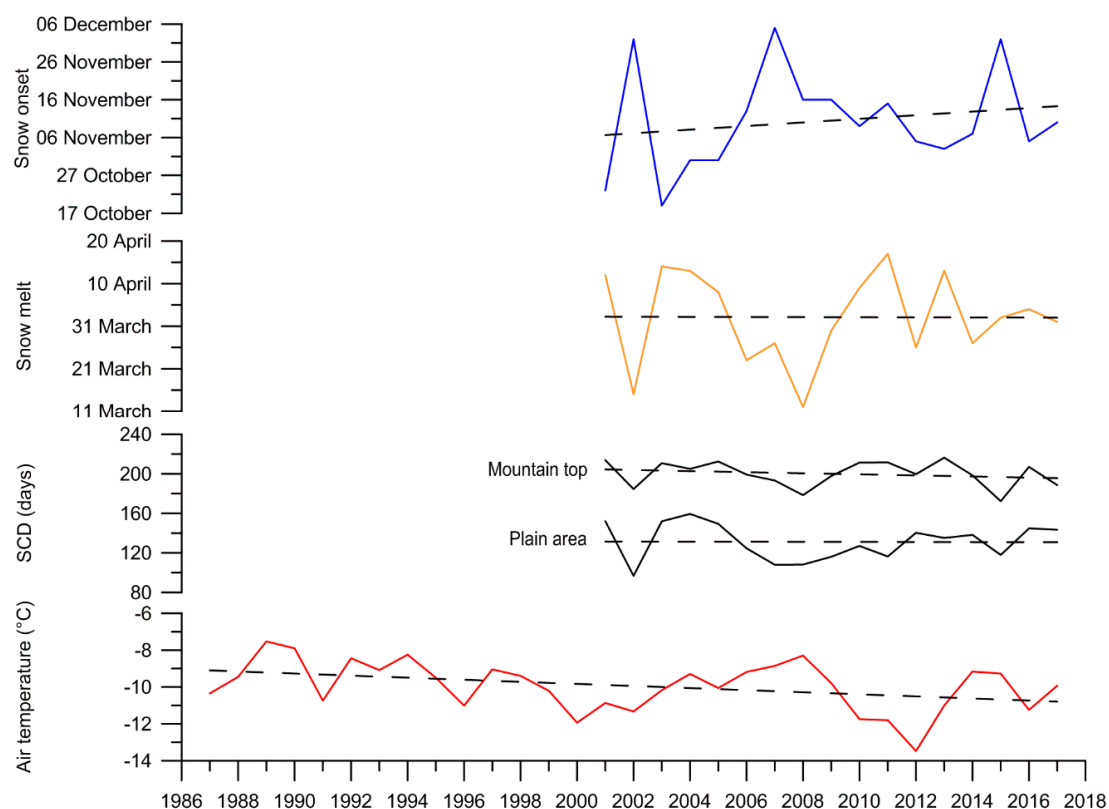


**Figure 7.** Trend analysis for the mean snow onset, snow melt, and SCD for 2001–2017, as well as monthly mean air temperature during snow season (ONDJFMA). Mountain peaks and plain areas were separated for SCD analysis. The temperature trend was analyzed using daily mean values from the nearest long-term observational site at the Chinggis Khan International Airport. There was no significant trend in each snow metric, while a slightly decreasing trend ( $p < 0.05$ ) in air temperature was detected during the snow season, including intermittent and persistent snow periods.

Interestingly, the monthly mean air temperature during the snow seasons, including intermittent and persistent snow periods, showed a decreasing trend over the last three decades. This decrease was statistically significant ( $p < 0.05$ ), but only for the mid-season months (DJF) (Table 2). Unlike in many regions in the world, a decrease or no increase in winter air temperature has been observed since the 1990s, replacing the general increasing trend since the 1960s over Central Asia under the influence of weakening SH [9,10,49]. The mean temperature of the snow season also showed an insignificant negative relationship ( $r^2 = 0.19$ ,  $p = 0.07$ ) with the SCD on the mountain top, indicating the decreasing temperature may have played an important role in preventing SCD decrease.

**Table 2.** The significance of trend analysis in monthly mean air temperature over the last 31 years at the Chinggis Khan International Airport (60 km from the study area).

	$r^2$	Slope	Intercept	p Value
October	0.002	−0.0092	−0.2744	0.78
November	0.053	−0.0721	−11.26	0.25
December	0.22	−0.142	−18.06	0.012 *
January	0.19	−0.14	−20.8	0.023 *
February	0.18	−0.15	−15.5	0.021 *
March	0.0009	−0.009	−7.82	0.09
April	0.03	0.0435	1.42	0.32

\* Significant, when  $p < 0.05$

### 3.3. Spatial Distribution of Snow

For analyzing the spatial distribution of snow in the study area, we exploited the high spatial resolutions of Landsat-7, Landsat-8, and Sentinel-2A images to create a sequence of snow cover maps during the snow season 2016/2017 (Figure S1, Supplementary Materials). The first snow covered area was captured on 11 October 2016 over mountain peaks by Landsat-7, and then decreased by 16 October after 5 days as captured by Sentinel-2 during the autumn transition period. The percent of SCA in the study area increased following several snow events and eventually reached 99.6% by 21 November, including the hydro-climatic station site (Figure 8). The persistency of seasonal snow cover for the Sugnugur catchment began after the heavy snow events from 6–7 November 2016.

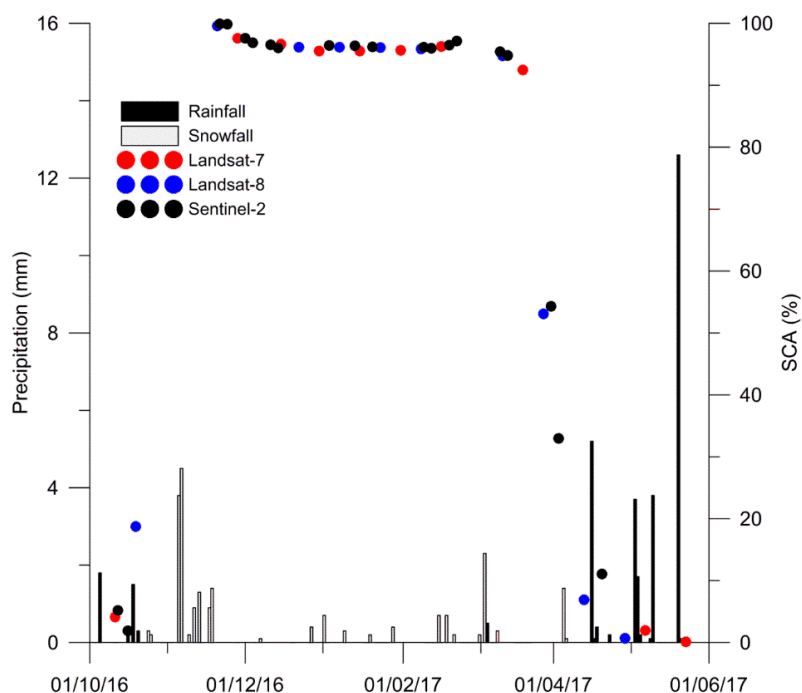


**Figure 8.** Precipitation events, distinguished as rain or snow, observed at the hydro-climatic station using the combination of albedo and air temperature measurements, and the inter-annual variability of SCA detected by different satellites over the Sugnugur catchment for winter 2016/2017.

We were able to use 28 images (70% of the total data) to identify the spatial distribution of seasonal persistent snow cover in 94.2% of the total area. The intermittent and snow free areas were 5.3% and 0.5% of the catchment area during the winter 2016/2017, respectively. The different spatial resolution of the two sensors may affect their combined use of time-series analysis [51] and result in minor uncertainties, mostly in the intermittent SCA. The intermittent snow areas appeared mostly on the steep south-facing slopes. Following several snow events, the south-facing slopes were covered by snow, but shortly became snow free due to higher sublimation rates or blowing-wind [52]. However, the intermittent SCD on the south-facing slopes still remain unclear because of the coarse spatial resolution of MODIS and non-daily coverage of the combined Landsat and Sentinel overpasses. The absence of snow cover on south-facing slopes was captured by our time-lapse camera, and was also visually inspected during the snow field campaigns (Figure S2 and Table S2, Supplementary Materials).

### 3.4. Mapping Snow Cover

Finally, we created a snow duration map (Figure 9) with 30 m resolution based on the findings that included the combination of both ground measurements and various optical remote sensing images. The map was produced only for seasonal persistent SCA because SCD for intermittent SCA had higher uncertainty. The simple correction, which was applied to Landsat and Sentinel images



using the supervised land-cover classification map, improved the spatial accuracy of SCA that was not detectable or often underestimated by MODIS satellites.

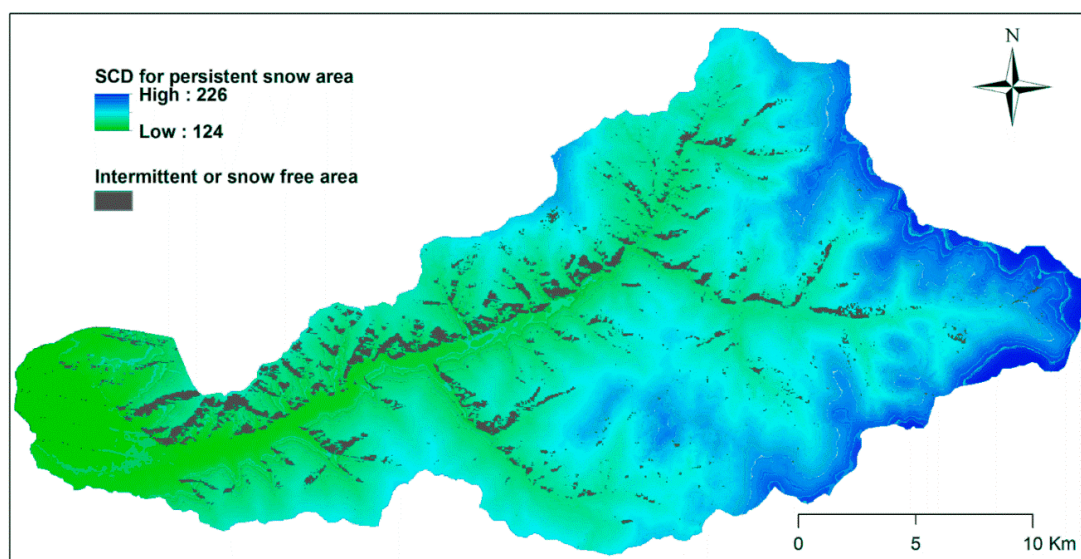


**Figure 9.** The total snow cover duration (SCD) days in Sugnugur catchment calculated only for persistent snow cover area. The intermittent and snow free areas were excluded due to their unknown snow accumulation periods.

The mean altitude-dependent SCD rate +6 days/100 m was consistent with that found in the same region [7]. The south-facing slopes were mostly snow free or with intermittent snow cover during winter due to high sublimation rate, wind blowing, and slope steepness. The mean annual SCD ranged from 124–226 days from the lowland plain area to the mountain peak (elevation difference of ~1700 m and horizontal distance of ~35 km), or showing high variability for such a small scale. Therefore, snow-melt water from the higher elevations with extended snow season is extremely important for balancing the Sugnugur River discharge during spring and autumn dry seasons.

To match our temporal record of snow depth observations at the hydro-climatic station, we compared the estimated SCD with the total observed SCD for the winters of 2012/2013 to 2016/2017. There was a clear underestimation of satellite derived SCD and resulted in an error of 12–13 days/year (Figure S3, Supplementary Materials). Previous studies have described MODIS snow products in clear-sky conditions to return high accuracies of >93% for Terra and >90% for Aqua [28,53]. Assuming these accuracies, our underestimation equates to 9% and is within the MODIS accuracy range. Nevertheless, errors are likely propagated through the relatively weak snow detection rate of MODIS sensors during the transition periods [13,54], the position of the hydro-climatic station relative to the receipt of incoming solar radiation, as well as the accuracy of annual altitude-dependent SCD rate.

The absence of snow cover on the south-facing slopes was captured by the automated time-lapse camera system, as well as was visually observed during fieldwork, which took place in the beginning of March 2017 and 2018, or the accumulated persistent snow cover period. The photographs from the camera showed a light snow event on 5 March 2017 together with the previous and following days, indicating the south-facing slopes were snow-free before the event (Figure S2, Supplementary Materials). The snow field measurements showed similar snow depths on both valley bottom and north-facing slope without any altitude-dependent increase. Therefore, we speculate that snow depth was homogeneous for the seasonal persistent SCA over the study area.

The days with below  $-1\text{ }^{\circ}\text{C}$  of  $T_s$  at the hydro-climatic station showed a positive relationship with the observed persistent SCD days. This suggests the possibility of validating the estimated SCD against the days with  $T_s < -1\text{ }^{\circ}\text{C}$  in the upper part of the catchment. For this analysis, surface temperature measurements at the valley bottom and north-facing slopes in different land-cover types were used



because the south-facing slopes were snow-free, and thus were excluded from the final SCD map. The estimated SCD determined from  $T_s$  revealed good agreement with an  $r^2$  of 0.85 ( $p < 0.001$ ) and a mean bias of  $\pm 1$  day compared to the hydro climatic station site. This would mean that the mean altitude-dependent SCD rate is consistent for persistent snow cover areas where MODIS snow data are contaminated by the topographic heterogeneity, forest, and shrubs.

#### 4. Discussion

Detection of snow from MODIS data has proven to exceed 90% accuracy on clear-sky days [44,48,53], but cloud coverage remains a major problem for all optical satellites. The temporal GF and CA (similar to those in [11,44]) applied to the MODIS data resulted in promising cloud reductions of up to 100%. This success is largely attributed to the SH, which enables a high number of clear-sky days over Mongolia (Figure 5). The obtained  $S_o$ ,  $S_m$ , and SCD did not indicate any significant trends since 2000, while mid-season winter (DJF) air temperature showed a decreasing trend over the last three decades (Figure 7) associated with the weakening of SH [8–10]. The SH starts to form in early autumn and causes early forming snow cover due to its contribution to changes in temperature and precipitation [6,8,9]. Therefore, the increased delay (statistically not significant) in  $S_o$  might be attributed to the seasonal strengthening of the SH. However, more detailed investigations on extreme weather and precipitation events in conjunction with the SH are necessary to draw strong conclusions.

In this study, we applied a simple alternative altitude-dependent correction to Landsat and Sentinel images to produce a time series of snow distribution in the Sugnugur catchment. Results showed the development of snow cover during the snow season in time and space and the classified seasonal intermittent and persistent SCAs (Figure 9). Classifying persistent SCA from intermittent SCA is important for more accurate hydrologic and water balance modelling. Since the temporal resolution of the produced snow maps from Landsat and Sentinel images is still coarse, SCD for intermittent SCA remains uncertain, and thus further investigations should also include the timing of intermittent snow cover where ground measurements are not available.

We also demonstrated the altitude-dependent SCD rate to be +6 days/100 m and is in good agreement with other rates across other Central Asian Mountains [7]. The overall accuracy of SCD was ~91% with the mean underestimation of ~12–13 days/year, which was probably caused by the reduced MODIS snow detection rate for thin occasional intermittent snow cover that occurs in autumn and spring months. The snow field measurements supported more comprehensive snow metrics, such as SWE and SD in the study area. In general, no changes in SD with increasing elevation were evident over the catchment. However, SD can vary at local scales because of forest interception, snow redistribution, as well as different sublimation rates [55], and it should be studied in future investigations.

As snow cover contributes to the surface energy balance [56], it appears that the daily mean surface temperature ( $T_s$ ) of  $< -1$  °C could be a good approximation of the overlaying existing persistent snow cover. Nevertheless, the applicability of using  $T_s$  for defining seasonal persistent SCD might be limited to certain spatial extents in cold regions because of the high climatic variability and characteristics of snow cover in the high altitudes and latitudes of the Northern Hemisphere. The  $T_s$  from iButtons also indicated that the changes in land-cover alter the timing of snow-melt processes, showing an earlier  $S_m$  in burned forest relative to unburned forest [57]. Therefore, the consequent effect of the earlier  $S_m$  in conjunction with energy exchange and long term snow monitoring, together with continuous river discharge measurement, should be discussed in further studies for observing the contribution of snow-melt water in the regional water resources.

#### 5. Conclusions

The detailed spatio-temporal distribution of snow has not been previously studied in Mongolia. In this study we examined snow cover in the Khentii Mountains, which is an important headwater for Lake Baikal and is the origin of the Selenga River. The use of multi-source data provided us essential information for understanding the timing and spatial characteristics of snow in the Sugnugur

catchment within a semi-arid climate where snow plays an important role in the regional water resources and surface energy balance.

The snow ground observation at the hydro-climatic station demonstrated strong variability in the timing of snow, especially during the intermittent snow cover period, showing a duration of 6–21 days/year, while persistent SCD was relatively stable with 132–141 days. Daily mean surface temperature of below  $-1$  °C with continuation of at least 14 days could give a good proxy of seasonal persistent snow cover. The manually measured SD at different elevations and land-cover types did not indicate any variability during the two consecutive snow field measurements.

The combined MODIS, Landsat, and Sentinel retrievals with various spatial and temporal resolutions gave us an opportunity to map snow cover and its duration in the mountainous region with 30 m resolution by applying a series of adjustments, including temporal gap-filling and conditional adjustments. The derived SCD rate is similar to that found in other Central Asian Mountains. The derived annual SCD shows high variations, but no significant trend since 2000. Overall, the combination of snow ground observation, field measurements, and high resolution open source optical remote sensing images with high temporal resolutions can be an option for understanding snow distribution and duration in mid-latitude mountain regions.

**Supplementary Materials:** The following are available online at <http://www.mdpi.com/2076-3263/9/1/53/s1>, Table S1. The acquisition dates of the satellite images that were used for producing the spatial distribution of snow. All selected images were taken on cloud-free conditions. Table S2. The overview of snow field measurements which were conducted on March 1, 2017 and 2018. Figure S1. Development of SCA for winter 2016–2017 from the combination of Landsat and Sentinel retrievals. The light-blue color indicates snow cover. Figure S2. Typical snow distribution in the Sugnugur catchment during the end of seasonal persistent snow cover period. Photographs were taken using a normal digital camera with automatic time-lapse setting. Figure S3. Anomalies of the estimated SCD for Terra and the combined version compared to the observed total SCD at the hydro-climatic station site for winters 2012/2013 to 2016/2017.

**Author Contributions:** M.M. analyzed the in situ and Landsat data, proposed the methodology, and wrote the manuscript. S.G. analyzed the MODIS and Sentinel data and contributed to the methodology and review. C.G.P. provided crucial suggestions and improved the manuscript writing. G.Y. and J.Y. carried out the snow field measurements. L.M. provided climatic data, supported the fieldwork, and supervised the study.

**Funding:** This research received no external funding.

**Acknowledgments:** Munkhdavaa Munkhjargal received funding from the Federal Ministry of Education and Research (BMBF) through the German Academic Exchange Service (DAAD) during the preparation of this manuscript. We acknowledge financial support by Deutsche Forschungsgemeinschaft within the funding programme Open Access Publishing, by the Baden-Württemberg Ministry of Science, Research and the Arts and by Ruprecht-Karls-Universität Heidelberg.

**Conflicts of Interest:** The authors declare no conflict of interest.

## Appendix A

**Table A1.** Abbreviations used in the paper and their explanation.

Abbreviation	Explanation	Unit
SCD	Snow cover duration	days
SCD RATE	Snow cover duration rate	day/m
SCA	Snow cover area	%
SWE	Snow water equivalent	mm
S <sub>O</sub>	Snow onset	date
S <sub>M</sub>	Snow melt	date
SH	Siberian high	-
DEM	Digital elevation model	m
GF	Gap-filling	-
CA	Conditional adjustment	-
NDSI	Normalized difference snow index	-
T <sub>A</sub>	Daily average air temperature	°C
T <sub>S</sub>	Daily average ground surface temperature	°C

## References

1. Wang, X.; Wu, C.; Wang, H.; Gonsamo, A.; Liu, Z. No evidence of widespread decline of snow cover on the Tibetan Plateau over 2000–2015. *Sci. Rep.* **2017**, *7*, 14645. [CrossRef] [PubMed]
2. Viviroli, D.; Dürr, H.H.; Messerli, B.; Meybeck, M.; Weingartner, R. Mountains of the world, water towers for humanity: Typology, mapping, and global significance. *Water Resour. Res.* **2007**, *43*, 1–13. [CrossRef]
3. Chevallier, P.; Pouyaud, B.; Mojaïsky, M.; Bolgov, M.; Olsson, O.; Bauer, M.; Froebrich, J. River flow regime and snow cover of the Pamir Alay (Central Asia) in a changing climate. *Hydrol. Sci. J.* **2014**, *59*, 1491–1506. [CrossRef]
4. Kim, Y.; Kimball, J.S.; Robinson, D.A.; Derksen, C. New satellite climate data records indicate strong coupling between recent frozen season changes and snow cover over high northern latitudes. *Environ. Res. Lett.* **2015**, *10*, 084004. [CrossRef]
5. Callaghan, T.V.; Johansson, M.; Brown, R.D.; Groisman, P.Y.; Labba, N.; Radionov, V.; Barry, R.G.; Bulygina, O.N.; Essery, R.L.H.; Frolov, D.M.; et al. The Changing Face of Arctic Snow Cover: A Synthesis of Observed and Projected Changes. *AMBIO* **2011**, *40*, 17–31. [CrossRef]
6. Bednorz, E.; Wibig, J. Circulation patterns governing October snowfalls in southern Siberia. *Theor. Appl. Climatol.* **2017**, *128*, 12–139. [CrossRef]
7. Zhou, H.; Aizen, E.; Aizen, V. Seasonal snow cover regime and historical change in Central Asia from 1986 to 2008. *Glob. Planet. Chang.* **2017**, *148*, 192–216. [CrossRef]
8. Cohen, J.; Foster, J.; Barlow, M.; Saito, K.; Jones, J. Winter 2009–2010: A case study of an extreme Arctic Oscillation event. *Geophys. Res. Lett.* **2010**, *37*. [CrossRef]
9. Cohen, J.; Screen, J.A.; Furtado, J.C.; Barlow, M.; Whittleston, D.; Coumou, D.; Francis, J.; Dethloff, K.; Entekhabi, D.; Overland, J.; et al. Recent Arctic amplification and extreme mid-latitude weather. *Nat. Geosci.* **2014**, *7*, 627–637. [CrossRef]
10. Panagiotopoulos, F.; Shahgedanova, M. Observed Trends and Teleconnections of the Siberian High: A Recently Declining Center of Action. *J. Clim.* **2005**, *18*, 1411–1422. [CrossRef]
11. Lindsay, C.; Zhu, J.; Miller, A.E.; Kirchner, P.; Wilson, T.L. Deriving Snow Cover Metrics for Alaska from MODIS. *Remote Sens.* **2015**, *7*, 12961–12985. [CrossRef]
12. Notarnicola, C.; Duguay, M.; Moelg, N.; Schellenberger, T.; Tetzlaff, A.; Monsorno, R.; Costa, A.; Steurer, C.; Zebisch, M. Snow Cover Maps from MODIS Images at 250 m Resolution. *Remote Sens.* **2013**, *5*, 110–126. [CrossRef]
13. Rittger, K.; Painter, T.H.; Dozier, J. Advances in Water Resources Assessment of methods for mapping snow cover from MODIS. *Adv. Water Resour.* **2013**, *51*, 367–380. [CrossRef]
14. Walters, R.D.; Watson, K.A.; Marshall, H.; Mcnamara, J.P.; Flores, A.N. A physiographic approach to downscaling fractional snow cover data in mountainous regions. *Remote Sens. Environ.* **2014**, *152*, 413–425. [CrossRef]
15. Gafurov, A.; Vorogushyn, S.; Farinotti, D.; Duethmann, D.; Merkushev, A.; Merz, B. Snow-cover reconstruction methodology for mountainous regions based on historic in situ observations and recent remote sensing data. *Cryosphere* **2015**, *9*, 451–463. [CrossRef]
16. Gurung, D.R.; Maharjan, S.B.; Shrestha, A.B.; Shrestha, M.S.; Bajracharya, S.R.; Murthy, M.S.R. Climate and topographic controls on snow cover dynamics in the Hindu Kush Himalaya. *Int. J. Climatol.* **2017**, *37*, 3873–3882. [CrossRef]
17. Liu, J.P.; Zhang, W.C. Long term spatio-temporal analyses of snow cover in Central Asia using ERA-Interim and MODIS products. *IOP Conf. Ser. Earth Environ. Sci.* **2017**, *57*, 012033. [CrossRef]
18. Manuel, G. An Operational Snow Cover Product from Sentinel-2 and Landsat-8 Data for Mountain Regions. *La Montagne, Territoire D'Innovation*; Grenoble, France, January 2017. Available online: <https://hal.archives-ouvertes.fr/halshs-01486820> (accessed on 9 January 2018).
19. Dedieu, J.; Carlson, B.Z.; Bigot, S.; Sirguey, P.; Vionnet, V.; Choler, P. On the Importance of High-Resolution Time Series of Optical Imagery for Quantifying the Effects of Snow Cover Duration on Alpine Plant Habitat. *Remote Sens.* **2016**, *8*, 481. [CrossRef]
20. Selkowitz, D.; Rittger, K. Developing a 30 m daily snow covered area time series for the Sierra Nevada Alpine using Landsat and MODIS data. In Proceedings of the AGU Fall Meeting, San Francisco, CA, USA, 3–7 December 2012.

21. Li, H.Y.; He, Y.Q.; Hao, X.H.; Che, T.; Wang, J.; Huang, X.D. Downscaling Snow Cover Fraction Data in Mountainous Regions Based on Simulated Inhomogeneous Snow Ablation. *Remote Sens.* **2015**, *7*, 8995–9019. [[CrossRef](#)]
22. Cristea, N.C.; Breckheimer, I.; Raleigh, M.S.; HilleRisLambers, J.; Lundquist, J.D. An evaluation of terrain-based downscaling of fractional snow covered area data sets based on LiDAR-derived snow data and orthoimagery. *Water Resour. Res.* **2017**, *53*, 6802–6820. [[CrossRef](#)]
23. Kostadinov, T.S.; Lookingbill, T.R. Remote Sensing of Environment Snow cover variability in a forest ecotone of the Oregon Cascades via MODIS Terra products. *Remote Sens. Environ.* **2015**, *164*, 155–169. [[CrossRef](#)]
24. Kopp, B.J.; Minderlein, S.; Menzel, L. Soil Moisture Dynamics in a Mountainous Headwater Area in the Discontinuous Permafrost Zone of northern Mongolia. *Arct. Antract. Alp. Res.* **2014**, *46*, 459–470. [[CrossRef](#)]
25. Kopp, B.J.; Lange, J.; Menzel, L. Effects of wildfire on runoff generating processes in northern Mongolia. *Reg. Environ. Chang.* **2016**, *17*, 1951–1963. [[CrossRef](#)]
26. Zhang, Y.; Mamoru, I.; Tetsou, O.; Dambaravja, O. Role of snow playing in water cycle in semi- arid region of Mongolia. In Proceedings of the 3rd International Workshop on Terrestrial Change in Mongolia, Tsukuba, Japan, 9–10 November 2004; pp. 23–24.
27. Wimmer, F.; Schlaffer, S.; aus der Beek, T.; Menzel, L. Distributed modelling of climate change impacts on snow sublimation in Northern Mongolia. *Adv. Geosci.* **2009**, *21*, 117–124. [[CrossRef](#)]
28. Parajka, J.; Holko, L.; Kostka, Z.; Blöschl, G. MODIS snow cover mapping accuracy in a small mountain catchment-comparison between open and forest sites. *Hydrol. Earth Syst. Sci.* **2012**, *16*, 2365–2377. [[CrossRef](#)]
29. Klein, A.G.; Barnett, A.C. Validation of daily MODIS snow cover maps of the Upper Rio Grande River Basin for the 2000–2001 snow year. *Remote Sens. Environ.* **2003**, *86*, 162–176. [[CrossRef](#)]
30. Tekeli, A.E.; Akyu, Z.; Arda, A.S.; Sensoy, A.; Sorman, Ü. Using MODIS snow cover maps in modeling snowmelt runoff process in the eastern part of Turkey. *Remote Sens. Environ.* **2005**, *97*, 216–230. [[CrossRef](#)]
31. Parajka, J.; Blöschl, G. Validation of MODIS snow cover images over Austria. *Hydrol. Earth Syst. Sci.* **2006**, *10*, 679–689. [[CrossRef](#)]
32. Ault, T.W.; Czajkowski, K.P.; Benko, T.; Coss, J.; Struble, J.; Spongberg, A.; Templin, M.; Gross, C. Validation of the MODIS snow product and cloud mask using student and NWS cooperative station observations in the Lower Great Lakes Region. *Remote Sens. Environ.* **2006**, *105*, 341–353. [[CrossRef](#)]
33. Wang, X.; Xie, H.; Liang, T. Evaluation of MODIS snow cover and cloud mask and its application in Northern Xinjiang, China. *Remote Sens. Environ.* **2008**, *112*, 1497–1513. [[CrossRef](#)]
34. Liang, T.; Zhang, X.; Xie, H.; Wu, C.; Feng, Q.; Huang, X.; Chen, Q. Remote Sensing of Environment Toward improved daily snow cover mapping with advanced combination of MODIS and AMSR-E measurements. *Remote Sens. Environ.* **2008**, *112*, 3750–3761. [[CrossRef](#)]
35. Huang, X.; Liang, T.; Zhang, X.; Guo, Z. Validation of MODIS snow cover products using Landsat and ground measurements during the 2001–2005 snow seasons over northern Xinjiang, China. *Int. J. Remote Sens.* **2011**, *32*, 133–152. [[CrossRef](#)]
36. Gafurov, A.; Kriegel, D.; Vorogushyn, S.; Merz, B. Evaluation of remotely sensed snow cover product in Central Asia. *Hydrol. Res.* **2013**, *44*, 506–522. [[CrossRef](#)]
37. Dong, C.; Menzel, L. Improving the accuracy of MODIS 8-day snow products with in situ temperature and precipitation data. *J. Hydrol.* **2016**, *534*, 466–477. [[CrossRef](#)]
38. Dong, C.; Menzel, L. Producing cloud-free MODIS snow cover products with conditional probability interpolation and meteorological data. *Remote Sens. Environ.* **2016**, *186*, 439–451. [[CrossRef](#)]
39. Dong, C. Remote sensing, hydrological modeling and in situ observations in snow cover research: A review. *J. Hydrol.* **2018**, *561*, 573–583. [[CrossRef](#)]
40. Hall, D.K.; Riggs, G.A. *MODIS/Terra Snow Cover Daily L3 Global 500 m Grid*, version 6; NASA National Snow and Ice Data Center Distributed Active Archive Center: Boulder, CO, USA, 2016.
41. National Aeronautic and Space Administration (NASA) and Ministry of Economy, Trade, and Industry (METI). *ASTER GDEM 2*; U.S Geological Survey: Sioux Falls, South Dakota, 2011. Available online: <https://earthexplorer.usgs.gov/> (accessed on 25 December 2017).
42. Landsat-7, Landsat-8 and Sentinel-2 (ESA) Image Courtesy of the U.S. Geological Survey. Available online: <https://earthexplorer.usgs.gov/> (accessed on 15 November 2017).
43. Hall, D.K.; Riggs, G.A.; Salomonson, V.V.; Digirolamo, N.E.; Bayr, K.J. MODIS snow-cover products. *Remote Sens. Environ.* **2002**, *83*, 181–194. [[CrossRef](#)]

44. Hall, D.K.; Riggs, G.A.; Foster, J.L.; Kumar, S.V. Development and evaluation of a cloud-gap-filled MODIS daily snow-cover product Part of the Physical Sciences and Mathematics Commons. *Remote Sens. Environ.* **2010**, *114*, 496–503. [[CrossRef](#)]
45. Wang, X.; Wang, J.; Jiang, Z.; Li, H.; Hao, X. An Effective Method for Snow-Cover Mapping of Dense Coniferous Forests in the Upper Heihe River Basin Using Landsat Operational Land Imager Data. *Remote Sens.* **2015**, *7*, 17246–17257. [[CrossRef](#)]
46. Ishikawa, M.; Iijima, Y.; Zhang, Y.; Kadota, T.; Yabuki, H.; Ohata, T.; Battogtokh, D.; Sharkhuu, N. Comparable energy balance measurements on the permafrost and immediate adjacent permafrost-free slopes at the southern boundary of Eurasian permafrost, Mongolia. In Proceedings of the Ninth International Conference on Permafrost, Fairbanks, AK, USA, 29 June–3 July 2008.
47. Hüsler, F.; Jonas, T.; Riffler, M.; Musial, J.P.; Wunderle, S. A satellite-based snow cover climatology (1985–2011) for the European Alps derived from AVHRR data. *Cryosphere* **2014**, *8*, 73–90. [[CrossRef](#)]
48. Liu, J.; Zhang, W.; Liu, T. Monitoring recent changes in snow cover in Central Asia using improved MODIS snow-cover products. *J. Arid Land* **2017**, *9*, 763–777. [[CrossRef](#)]
49. Hu, Z.; Zhang, C.; Hu, Q.; Tian, H. Temperature Changes in Central Asia from 1979 to 2011 Based on Multiple Datasets. *J. Clim.* **2014**, 1143–1167. [[CrossRef](#)]
50. Dietz, A.J.; Keunzer, C.; Conrad, C. Snow-cover variability in Central Asia between 2000 and 2001 derived from improved MODIS daily snow-cover products. *Int. J. Remote Sens.* **2013**, *34*, 3879–3902. [[CrossRef](#)]
51. Mandanici, E.; Bitelli, G. Preliminary Comparison of Sentinel-2 and Landsat 8 Imagery for a Combined Use. *Remote Sens.* **2016**, *8*, 1014. [[CrossRef](#)]
52. Revuelto, J.; Gilaberte, M. The effect of slope aspect on the response of snowpack to climate warming in the Pyrenees. *Theor. Appl. Climatol.* **2014**, *117*, 207–219.
53. Hall, D.K.; Riggs, G.A. Accuracy assessment of the MODIS snow products. *Hydrol. Process.* **2007**, *21*, 1534–1547. [[CrossRef](#)]
54. Pu, Z.; Xu, L.; Salomonson, V.V. MODIS/Terra observed seasonal variations of snow cover over the Tibetan Plateau. *Geophys. Res. Lett.* **2007**, *34*, L067606. [[CrossRef](#)]
55. Woo, M.; Marsh, P. Snow, frozen soils and permafrost hydrology in Canada, 1999–2002. *Hydrol. Process.* **2005**, *19*, 215–229. [[CrossRef](#)]
56. Zhang, T. Influence of the seasonal snow cover on the ground thermal regime: An overview. *Rev. Geophys.* **2005**, *43*, RG4002. [[CrossRef](#)]
57. Burles, K.; Boon, S. Snowmelt energy balance in a burned forest plot, Crowsnest Pass, Alberta, Canada. *Hydrol. Process.* **2011**, *25*, 3012–3029. [[CrossRef](#)]



© 2019 by the authors. Licensee MDPI, Basel, Switzerland. This article is an open access article distributed under the terms and conditions of the Creative Commons Attribution (CC BY) license (<http://creativecommons.org/licenses/by/4.0/>).